A New Method for Detection of Cirrus Overlapping Water Clouds and Determination of Their Optical Properties

FU-LUNG CHANG

Earth System Science Interdisciplinary Center, University of Maryland, College Park, College Park, Maryland

ZHANQING LI

Earth System Science Interdisciplinary Center, and Department of Atmospheric and Oceanic Science, University of Maryland, College Park, College Park, Maryland

(Manuscript received 3 December 2004, in final form 21 March 2005)

ABSTRACT

The frequent occurrence of high cirrus overlapping low water cloud poses a major challenge in retrieving their optical properties from spaceborne sensors. This paper presents a novel retrieval method that takes full advantage of the satellite data from the Moderate Resolution Imaging Spectroradiometer (MODIS). The main objectives are identification of overlapped high cirrus and low water clouds and determination of their individual optical depths, top heights, and emissivities. The overlapped high cloud top is determined from the MODIS CO_2-slicing retrieval and the underlying low cloud top is determined from the neighboring MODIS pixels that are identified as single-layer low clouds. The algorithm applies a dual-layer cloud radiative transfer model using initial cloud properties derived from the MODIS CO_2-slicing channels and the visible (0.65 μm) and infrared (11 μm) window channels. An automated iterative procedure follows by adjusting the high cirrus and low water cloud optical depths until computed radiances from the dual-layer model match with observed radiances from both the visible and infrared channels. The algorithm is valid for both single-layer and dual-layer clouds with the cirrus optical depth $<\sim 4$ (emissivity $<\sim 0.85$). For more than two-layer clouds, its validity depends on the thickness of the upper-layer cloud. A preliminary validation is conducted by comparing against ground-based active remote sensing data. Pixel-by-pixel retrievals and error analyses are presented. It is demonstrated that retrievals based on a single-layer assumption can result in systematic biases in the retrieved cloud top and optical properties for overlapped clouds. Such biases can be removed or lessened considerably by applying the new algorithm.

1. Introduction

To date, the overlap of high cirrus cloud and low water cloud has posed a major challenge in determining cloud optical properties using passive weather satellite observations. Presence of cirrus overlapping low cloud has been frequently reported by surface observers and aircraft observations (Hahn et al. 1982, 1984; Warren et al. 1985; Tian and Curry 1989). Based on a 12-yr (1965–76) dataset of ship-reported synoptic observations over the North Atlantic Ocean between 30° and 60°N, Hahn et al. (1982) found that out of all cirrus clouds observed, the probability of the coexistence of stratus and cirrus clouds was greater than 50%. Tian and Curry (1989) found that the probability of the coexistence of stratus and cirrus clouds was more than 60%, based on the Air Force Global Weather Central nephanalysis data during 1979 over the North Atlantic Ocean between 40° and 60°N. None of these data provide cloud optical depth and top height information, which is important for understanding cloud–radiation interactions and computing heating rates in the atmosphere.

Identification of overlapped clouds and determination of their optical properties can be achieved by combining ground-based active sensors like radar and lidar (Mace et al. 2001; Clothiaux et al. 2000). Unfortunately, such ground-based remote sensing data are only available from a very small number of stations around the world. The longest continuous record of observations has been made at three major sites of the U.S. Depart-

Corresponding author address: Dr. Fu-Lung Chang, Earth System Science Interdisciplinary Center, 2207 Computer and Space Sciences Bldg., University of Maryland, College Park, College Park, MD 20742-2465.
E-mail: fchang@essic.umd.edu

ment of Energy's Atmospheric Radiation Measurement (ARM) Program (Ackerman and Stokes 2003). Given the high frequency of occurrence of overlapped clouds, satellite remote sensing is essential in observing such cloud configurations on a global scale.

Different methods have been proposed to identify multilayer clouds using passive satellite observations. Baum et al. (1995) applied a CO_2-slicing technique to the high-resolution infrared radiation sounder (HIRS) data to determine high cirrus clouds and used 11-μm data from the collocated Advanced Very High Resolution Radiometer (AVHRR) data to determine the presence of low clouds. Baum and Spinhirne (2000) proposed a bispectral clustering method to identify areas containing an overlapped cloud system using 1.6- and 11-μm data from the Moderate Resolution Imaging Spectroradiometer (MODIS) Airborne Simulator (MAS). Ou et al. (1996) developed a threshold test scheme to distinguish AVHRR pixels that contain overlapped and nonoverlapped clouds. Baum et al. (1997) also used AVHRR data and developed a fuzzy logic scheme to determine pixels with overlapped cloud layers. Pavolonis and Heidinger (2004) further developed two threshold test schemes for detecting multilayer cloud pixels, one scheme for AVHRR and the other scheme for National Polar-orbiting Operational Environmental Satellite System (NPOESS). All of these methods were focused on the detection of overlapped clouds and not on the retrieval of their optical properties.

Gonzalez et al. (2002) used multiangle satellite measurements from the Along-Track Scanning Radiometer (ATSR) to determine the cloud optical depth and effective particle size of cirrus clouds overlying thick water clouds. Their retrievals assumed constant high and low cloud-top heights. Combinations of microwave, infrared (IR), and visible (VIS) measurements have been used to retrieve overlapped cloud properties (Sheu et al. 1997; Lin et al. 1998; Ho et al. 2003), but they were restricted to high thick clouds over ocean only.

Global cloud climatologies have been generated using data from the International Satellite Cloud Climatology Project (ISCCP; Rossow and Schiffer 1991, 1999) and the MODIS (King et al. 2003; Platnick et al. 2003). The ISCCP scheme relies essentially on an IR channel ($\sim$11 μm) to retrieve cloud-top altitude and a VIS channel ($\sim$0.6 μm) to retrieve cloud optical depth. Both channels are commonly available in all weather satellite sensors. Given that most high cirrus clouds are semitransparent (Liou 1986), the IR-measured brightness temperatures are influenced significantly by the underlying surface and/or low clouds that are generally much warmer than the cirrus cloud temperatures. To account for the cirrus transmissivity, an attempt was made to correct the retrievals of cirrus cloud-top height using optical depths retrieved from the VIS channel (Rossow and Schiffer 1999). This may alleviate the problem but cannot solve it because of fundamental limits in the information content of the two channels. For thin cirrus overlapping thick low clouds, the low clouds overwhelm the signal in the VIS channel.

For MODIS, cirrus cloud-top heights are retrieved using data from the partially absorbing multispectral infrared channels near the 15-μm CO_2 absorption bands. The scheme is known as the CO_2-slicing technique that was previously applied to the visible infrared spin scan radiometer (VISSR) Atmospheric Sounder (VAS) and HIRS data (Chahine 1974; Smith and Platt 1978; Wielicki and Coakley 1981; Wylie and Menzel 1989; Menzel et al. 1992; Baum and Wielicki 1994; Baum et al. 1995; Wylie et al. 1994; Jin et al. 1996; Wylie and Menzel 1999). Given that the satellite view is from space, clouds with the highest cloud tops in the atmosphere are preferentially detected. Since the CO_2-slicing technique is very sensitive in detecting thin cirrus clouds at the highest altitude, most low clouds underlying the high thin clouds are obscured and neglected. However, the VIS-retrieved cloud optical depths can be overwhelmed by low cloud signals. These cirrus overlapping low clouds would be misidentified as thick high clouds.

A promising tool to deal with this problem is the use of spaceborne cloud radars such as the CloudSat, currently scheduled for launch in late 2005 (Stephens et al. 2002). Because this sensor only provides measurements at a single nadir point of view, it will take time to amass enough samples to develop a meaningful global climatology of cloud vertical structure. Maximal exploitation of the conventional passive imaging sensors is thus highly desirable, which motivated this investigation. A more useful approach would be the combination of passive data from the MODIS and active radar data from CloudSat. This can be achieved because the two sensors will fly one after another in the same orbit (Stephens et al. 2002).

By virtue of the multispectral channels available from the MODIS on *Terra* (started operation in 2000) and *Aqua* (started operation in 2002) satellites, this paper presents a new method that can 1) detect overlapped high and low clouds on a pixel-level basis, and 2) determine the optical depths and heights for the individual high and low clouds. The method combines the MODIS CO_2-slicing technique with traditional IR and VIS techniques to overcome some limitations due to single-layer cloud assumptions used by conventional satellite cloud retrieval methods. Preliminary compari-

sons are made against ground-based active remote sensing data (Clothiaux et al. 2000; Mace et al. 2001) obtained at the ARM Southern Great Plains (SGP) site in north-central Oklahoma.

In section 2, the rationale for identifying overlapped clouds is presented. Section 3 describes our new overlapping cloud identification and retrieval algorithm and corresponding radiative transfer calculations. Section 4 presents analyses of the retrievals, uncertainties, and validation against ground-based retrievals and other operational single-layer algorithms. Section 5 gives the concluding remarks.

2. Rationale for identifying overlapped cloud systems

Fundamental information concerning the presence of overlapped clouds in the MODIS product (collection 4) is obtained by combining information from the CO_2-slicing channels and the VIS and IR window channels. In the MODIS operational products, cloud-top pressure and temperature (PC and TC) are estimated from the MODIS CO_2-slicing retrieval algorithm (Menzel et al. 1992; Menzel et al. 2002) for cirrus clouds, and from the 11-μm channel for low clouds. Cloud optical depth is estimated from a VIS channel, that is, 0.65 μm for land and 0.86 μm for ocean (Platnick et al. 2003).

Figure 1 illustrates the information contained in two *Terra*/MODIS granules (5-min segments of two satellite passes). The images include the 0.65-μm VIS reflectance (Figs. 1a,d), the 11-μm IR brightness temperature (Figs. 1b,e), and the MODIS-retrieved TC (Figs. 1c,f) product (MOD06, collection 4). One granule was acquired at 1715 UTC 2 April 2001 (Figs. 1a–c) and another at 1735 UTC 6 March 2001 (Figs. 1d–f). Each granule covers an area of approximately 4000 km $\times$ 4000 km with the part of the ARM SGP site marked by the boxed area (centered at 36.6°N, 97.5°W). In the images, clouds appear brighter with large 0.65-μm reflectances and cold 11-μm brightness temperatures. The MODIS TC image exhibits more high cold clouds from the CO_2-slicing retrieval than what is revealed by the 11-μm brightness temperature.

The CO_2-slicing method is more accurate in determining cloud-top altitudes for midlevel to high clouds (especially semitransparent cirrus clouds) than the conventional IR method (Wylie and Menzel 1989; Menzel et al. 1992; Jin et al. 1996). Wylie and Menzel (1989) showed that the CO_2-slicing cloud-top heights derived from the VAS data over North America were within a 40-hPa rms of the cloud-top heights inferred from radiosonde moisture profiles and from satellite stereo parallax measurements, but were 70 hPa lower on average than the lidar measurements.

The MODIS algorithm utilizes four partial CO_2-absorption channels (nominally at 13.3, 13.6, 13.9, and 14.2 μm), along with the 11-μm window channel to retrieve an effective cloud-top altitude. The resulting TC represents the top of the highest cloud seen from space, while the 11-μm brightness temperature represents infrared emission, which is dictated by both cloud-top height and optical depth. Note that the brightness temperature is not a physical cloud temperature, but a simple transformation of thermal radiance into temperature.

Figure 2 shows the comparisons of the two temperatures and the 0.65-μm retrieved cloud column optical depth (τ_{VIS}) obtained from the boxed area ($\sim 100 \times 100$ km^2) over the ARM SGP central facility (CF) site, as shown in Figs. 1a–c. In Fig. 2a, MODIS TCs less than 250 K are from the CO_2-slicing retrievals that reveal the presence of high cold clouds. Their corresponding 11-μm brightness temperatures are much warmer at around 270 K. The differences between the warm 11-μm brightness temperatures and cold CO_2-slicing TC indicate the presence of high thin cirrus clouds. For low clouds, the MODIS TCs are generally around 280 K with similar 11-μm brightness temperatures. From the 11-μm brightness temperature alone, it is difficult to detect any high thin cirrus cloud.

Figure 2b plots MODIS TCs as a function of 0.65-μm retrieved τ_{VIS}. In general, τ_{VIS} has very large values (>10) for both high cold pixels (TC $<$ 250 K) and low warm pixels (TC $>$ 270 K). Without other information, the cold TC associated with large τ_{VIS} would be interpreted as high thick clouds when they are, in fact, optically thick low and warm clouds overlapped by thin, cold cirrus clouds. The two types of cloud have completely different radiative effects and heating profiles. High thick clouds have small net radiative forcing, but large positive and negative forcings for the longwave and shortwave components, respectively. For thin cirrus overlapping thick low clouds, the shortwave cooling dominates over the longwave warming so the cloud system has a net strong cooling. Their heating profiles also differ considerably, leading to different thermodynamic and dynamic atmospheric conditions. In light of the frequent occurrence of cirrus overlapping low clouds (Hahn et al. 1982, 1984; Warren et al. 1985; Tian and Curry 1989), use of a single-layer cloud model for remote sensing of all clouds would incur large uncertainties in retrieving their optical properties.

3. Algorithm

The retrieval algorithm presented here concentrates on semitransparent high cirrus clouds (i.e., emissivity $<$

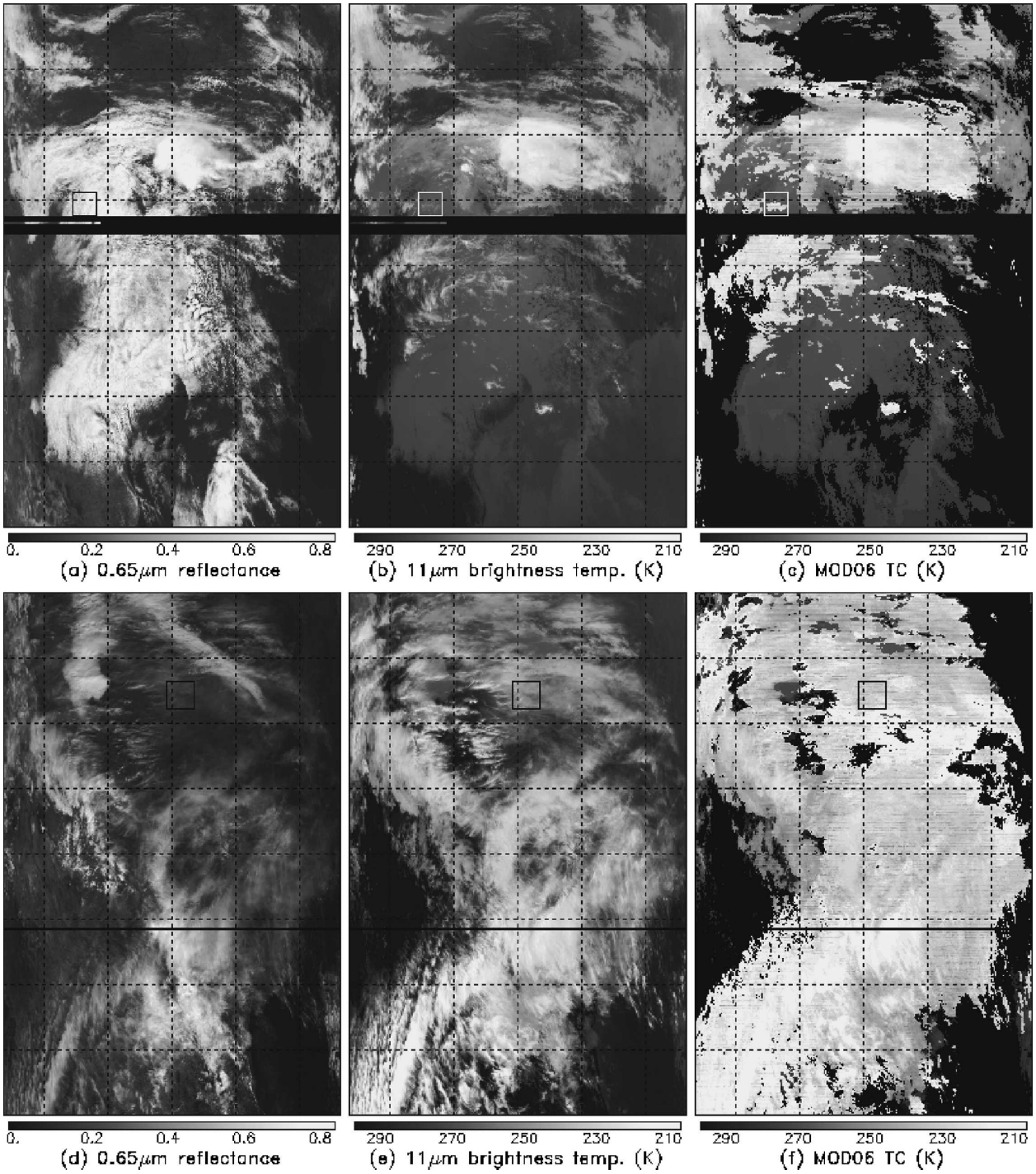

FIG. 1. MODIS granule images (5-min orbital passes ~1350 × 2000 pixels) of the (a), (d) 0.65-μm reflectance, (b), (e) 11-μm brightness temperature (K), and (c), (f) MOD06 TC (K) acquired on (a)–(c) 1715 UTC 2 Apr and (d)–(f) 1735 UTC 6 Mar 2001. The boxed area ~$(100\ \text{km})^2$ is centered on the ARM SGP site (36.6°N, 97.5°W). Dashed lines are for every 250 × 250 pixels.

0.85 and PC < 500 hPa). The criteria encompass the majority of cirrostratus and cirrocumulus clouds (Comstock and Sassen 2001; Sassen et al. 2003). The main objectives are 1) to determine whether or not an underlying low cloud is present and 2) to retrieve the cirrus and low cloud properties separately if the cirrus cloud overlaps with a low cloud.

The essential pieces of information used in our

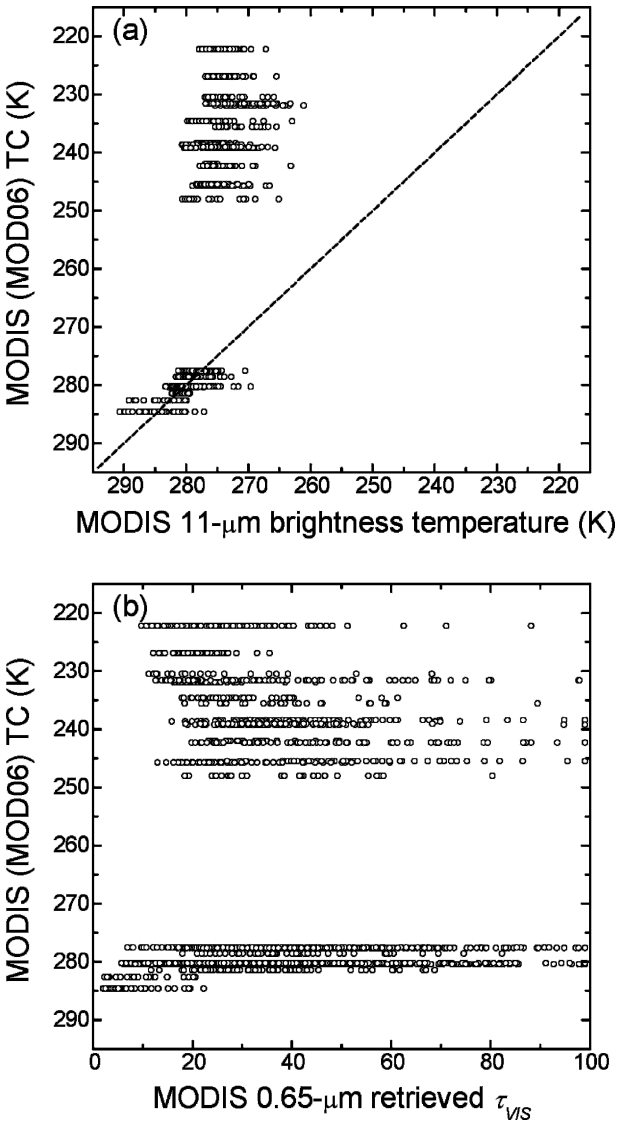

FIG. 2. (a) MODIS (MOD06) TC vs the 11-μm brightness temperature and (b) MODIS TC vs the 0.65-μm retrieved τ_{VIS} for the boxed area shown in Figs. 1a–c.

method include: 1) a high cloud (hc subscripts) PC/TC (P_{hc}/T_{hc}) estimated from the CO_2-slicing retrieval (Menzel et al. 1992; Menzel et al. 2002); 2) an underlying low cloud (lc) PC/TC (P_{lc}/T_{lc}) estimated from nearby low cloud pixels using the 11-μm retrieval method (Platnick et al. 2003); 3) a high cloud optical depth estimated from an effective IR emissivity (Platt and Stephens 1980; Minnis et al. 1990); and 4) a total-column cloud optical depth estimated from the retrieval at a VIS channel (Platnick et al. 2003), which contains both signals from the overlapped cirrus and low cloud.

Figure 3 shows a flowchart illustrating our algorithm for identifying and retrieving both single-layer and dual-layer high clouds. For all high cloud pixels with a $P_{hc} < 500$ hPa, it begins with two estimates of cloud VIS optical depths, that is, τ_{VIS} and τ'_{VIS}, from single-layer cloud model. Here, τ_{VIS} is retrieved from the VIS reflectance following the traditional bispectral VIS–IR retrieval method like that used in ISCCP; and τ'_{VIS} is inferred from the IR effective emissivity using CO_2-slicing T_{hc} and 11-μm radiance, which is described as follows. It first uses the operational MODIS IR effective emissivity (ε_{IR}) that is computed by assuming a single-layer overcast high cloud (Menzel et al. 1992; Wylie et al. 1994; Menzel et al. 2002):

$$\varepsilon_{IR} = \frac{R - R_{clr}}{R_{hc} - R_{clr}}, \tag{1}$$

where R is the MODIS-observed 11-μm radiance, R_{hc} is the simulated high cloud 11-μm blackbody radiance using the MODIS CO_2-slicing T_{hc}, and R_{clr} representing the clear-sky background 11-μm radiance.

A cloud optical depth in the IR region, τ_{IR}, is then estimated from ε_{IR} (Platt and Stephens 1980; Minnis et al. 1990),

$$\tau_{IR} = -\mu \ln(1 - \varepsilon_{IR}), \tag{2}$$

where μ denotes the cosine of the satellite zenith angle. This τ_{IR} is then converted to cloud optical depth in the VIS region, τ'_{VIS}, using a parameterization scheme (Minnis et al. 1990; Rossow and Schiffer 1999)

$$\tau'_{VIS} = \xi \tau_{IR}, \tag{3}$$

where the ratio ξ is taken to be 2.13 for ice clouds and 2.56 for water clouds (Minnis et al. 1993a; Rossow and Schiffer 1999). Note that the estimation of τ_{IR} from ε_{IR} neglects the scattering effect at IR wavelengths. The computed τ_{IR} thus represents the absorption optical depth and is slightly less than the total extinction optical depth, whose mean bias should be no more than 10% (Platt and Stephens 1980; Minnis et al. 1993a). The ratio depends on cloud particle phase, size, and shape distribution (Minnis et al. 1993a).

For semitransparent cirrus cloud ($\varepsilon_{IR} < 0.85$), the IR-converted τ'_{VIS} represents the effective cirrus optical depth influenced by cloud-top height. As such, we can compare τ'_{VIS} to the total-column τ_{VIS} retrieved from the VIS channel to detect overlapped clouds. For a thin cirrus that overlaps a low water cloud, τ'_{VIS} is significantly smaller than τ_{VIS}. This is because τ'_{VIS} is dictated by the IR emission of the column through R and the cloud-top temperature of the thin cirrus through R_{hc}, whereas τ_{VIS} is dominated by the low thick cloud. On the contrary, for single-layer cirrus cloud τ'_{VIS} and τ_{VIS} are similar because both are dominated by cirrus cloud only. Figure 4 shows the comparisons between τ'_{VIS} and τ_{VIS} for the two cloud cases obtained at the ARM SGP

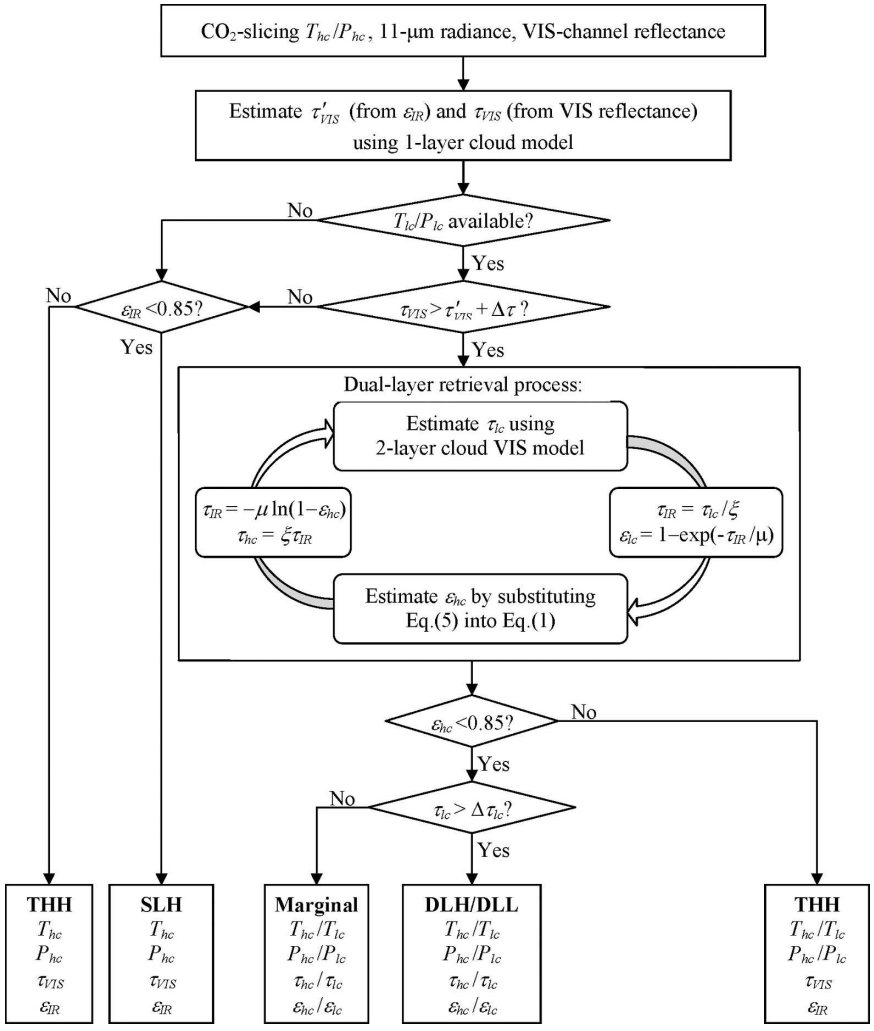

FIG. 3. Schematic flowchart diagram for illustrating the retrieval algorithm. Cloud type classifications are shown in bold. The retrieved cloud properties corresponding to each cloud type are also indicated.

site as indicated by the boxed areas shown in Fig. 1. The comparisons are made for MODIS pixels with a CO_2-slicing TC < 500 hPa and obtained on 2 April 2001 (Fig. 4a) and 6 March 2001 (Fig. 4b), respectively. Two different clusters are clearly seen, $\tau_{VIS} \gg \tau'_{VIS}$ in Fig. 4a and $\tau_{VIS} \sim \tau'_{VIS}$ in Fig. 4b, which are separated by a dotted curve plotting the function of $\tau_{VIS} = \tau'_{VIS} + \Delta\tau$, where $\Delta\tau$ is set to 1.5. It accounts for the uncertainties of potential errors in the retrievals of both τ_{VIS} and τ'_{VIS} that are discussed later. In Fig. 4b, the two optical depths are highly correlated with a coefficient $\rho_{cor} = 0.81$. The correlation would be better without the presence of a few scattered points where $\tau_{VIS} \ll \tau'_{VIS}$. The small τ_{VIS} may be caused by the overestimation of the surface albedo and/or the overestimation of τ'_{VIS} due to the overestimation of ε_{IR}. With reference to the ARM ground-based radar and lidar observations, the two clusters were found to correspond to a cirrus overlapping water cloud system (Fig. 4a) and a single-layer cirrus cloud system (Fig. 4b), respectively. Therefore, differences between the two optical depths are used to decide if a dual-layer cloud model should be invoked to refine the retrievals.

For an overlapped cloud case, the initial estimate of ε_{IR} from Eq. (1) needs to be modified for correcting the emission from the lower cloud. This is achieved by replacing R_{clr} in Eq. (1) with an adjusted radiance term R' given by

$$R' = \varepsilon_{lc}R_{lc} + (1 - \varepsilon_{lc})R_{clr}, \quad (4)$$

where R_{lc} is the simulated low cloud 11-μm blackbody radiance at T_{lc}, and ε_{lc} is the low cloud 11-μm emissivity

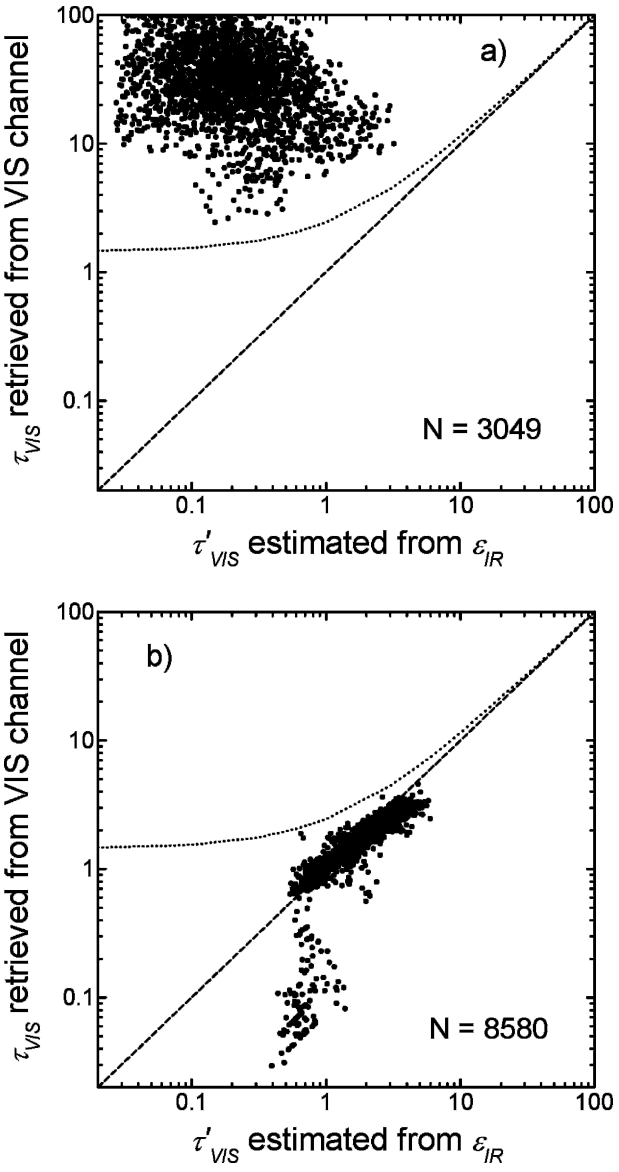

FIG. 4. Comparisons of τ_{VIS} (retrieved from the VIS channel) and τ'_{VIS} (estimated from ε_{IR}) as plotted in logarithmic scales. The data are obtained for high cloud pixels with PC $<$ 500 hPa from the boxed area as shown in Fig. 1, for (a) 2 Apr (Figs. 1a–c) and (b) 6 Mar 2001 (Figs. 1d–f). The diagonal dashed lines are the one-to-one lines. The dotted lines are for $\tau_{VIS} = \tau'_{VIS} + \Delta\tau$, where $\Delta\tau$ is for the margin of uncertainties.

to be determined from the retrieved low cloud optical depth (τ_{lc}). To estimate the two quantities, it is necessary to know the cloud-top height of the lower cloud. Assuming that the low clouds in nearby regions are from the same cloud system, single-layer low clouds are searched before applying the dual-layer retrieval. The search begins with adjacent pixels immediately next to the cirrus pixel. If no adjacent low cloud pixel is obtained, an average is derived of the low-cloud-top property from a neighboring area of ±125 km, which is comparable to a typical GCM grid size and a typical mesoscale cloud scale. In case of absence of any single-layer low cloud property in the searched area, no overlap retrieval will be applied.

When all three conditions are met, that is, PC $<$ 500 hPa, $\tau_{VIS} > \tau'_{VIS}$ and neighboring low cloud information available, the dual-layer cloud algorithm is applied to retrieve τ_{lc} for the underlying low cloud. The retrieval is based on the VIS radiative transfer calculations for a dual-layer cloud system consisting of a high ice cloud layer and a low water cloud layer. Initially, the ε_{IR}-based τ'_{VIS} is used as an input to the two-layer model. A best fit value of τ_{lc} is retrieved by adjusting τ_{lc} until the model-computed VIS reflectance matches the observation. The next step is to convert τ_{lc} at the VIS channel to its corresponding low cloud τ_{IR} at the IR channel using Eq. (3). Likewise, Eq. (2) is applied to compute ε_{lc} for the low cloud based on the retrieved τ_{IR}. Substituting Eq. (4) into Eq. (1) for R_{clr}, a nominal high cirrus cloud ε_{hc} can be derived by

$$\varepsilon_{hc} = \frac{R - R'}{R_{hc} - R'}. \tag{5}$$

A nominal high cirrus cloud optical depth (τ_{hc}) is obtained following Eqs. (2) and (3). Because the retrievals of τ_{hc} and τ_{lc} are mutually dependent, an iterative retrieval process is needed as illustrated in Fig. 3. The retrieved τ_{hc} and τ_{lc} usually converge after two iterations because τ_{lc} is often large enough so that ε_{lc} is near unity.

All high clouds with PC $<$ 500 hPa are classified into three major categories, namely, 1) single-layer cirrus cloud (SLH), 2) cirrus overlapping low cloud (DLH), and 3) thick high clouds (THH; $\varepsilon_{hc} \geq 0.85$). The SLH and DLH categories are retrieved only for $\varepsilon_{hc} < 0.85$. A dual-layer low (DLL) cloud category is simultaneously retrieved with DLH for the overlapped low clouds. A marginal category accounting for the uncertainties in the algorithm is also included if the retrieved τ_{lc} is smaller than a threshold value ($\Delta\tau_{lc}$) that is determined because of our assumptions made in the radiative transfer calculations as described later. The THH category includes two processing paths with (rightmost path) and without (leftmost path) information on nearby low clouds. In either case, the THH cloud is considered as a single thick layer with a given total-column τ_{VIS}. The THH clouds associated with nearby low cloud P_{lc}/T_{lc} information are probably overlapped. Note that because of instrument noise, the minimum of ε_{hc} and τ_{hc} retrievals is ~0.01. The CO_2-slicing algorithm may miss roughly half of the thin cirrus with $\varepsilon_{hc} < 0.1$ that ac-

counts for about 5% of the observations of high cloud (Menzel et al. 2002).

For all lower clouds with PC $\geq$ 500 hPa, no decision was made regarding cloud overlapping. They are referred to as single-layer low (SLL) clouds with a total-column τ_{lc} retrieved from the VIS channel. So, it is likely that clouds having more than two layers are classified as dual-layer by the algorithm. Cloud overlapping as viewed from an oblique angle may be identified as DLH, although they may not overlap in the vertical plane.

The dual-layer retrieval process is actually performed by means of lookup tables. Radiance lookup tables are generated by running an adding–doubling code (Chang and Li 2002) for various combinations of a two-layer cloud model with overlapped ice and water clouds. The radiances are simulated at 32-stream Gauss quadrature points in zenith angles and 11 relative azimuth angles at 0°, 10°, 30°, 50°, 70°, 90°, 110°, 130°, 150°, 170°, and 180°. The input values for high clouds are τ_{hc} = 0.01, 0.25, 0.5, 1, 2, 3, and 5 and P_{hc} = 100, 300, and 500 hPa. For low clouds, they are τ_{lc} = 0.05, 0.25, 1, 2, 3, 4, 6, 8, 12, 16, 24, 32, 40, 48, 56, 64, 80, and 100 and P_{lc} = 500, 700, 900, and 1000 hPa. The atmosphere is divided into ten vertical layers with each layer thickness equal to 100 hPa. The high and low cloud layers are inserted at each PC level as an infinitesimal plane-parallel layer.

Our microphysical model for the high clouds assumes an ice cloud layer with a fixed effective radius r_e = 30 μm and adopts the scattering phase functions of the fractal polycrystal model (Macke 1993; Mishchenko et al. 1996). This ice cloud model adopted is the same as in the ISCCP (Rossow and Schiffer 1999). It generally agrees well with the observational data (Minnis et al. 1993b; Francis 1995; Descloitres et al. 1998). Descloitres et al. (1998) show that the observed angular distributions of the visible reflectances from cirrus clouds agree within a few percent with calculations based on the fractal-polycrystal scattering phase functions. The VIS optical refractive indices used for the ice cloud are $1.332 + 1.672 \times 10^{-8}i$ for 0.65 μm and $1.329 + 3.290 \times 10^{-7}i$ for 0.86 μm (Warren 1984). Our microphysical model for the low clouds assumes a water cloud layer with a fixed r_e = 10 μm and Mie scattering phase functions. The optical refractive indices used for water clouds are $1.332 + 1.672 \times 10^{-8}i$ for 0.65 μm and $1.329 + 3.290 \times 10^{-7}i$ for 0.86 μm (Hale and Querry 1973). The assumptions made concerning the cloud microphysical models may incur uncertainties in the retrieved optical depths on the order of 30%–50% for thin cirrus clouds (Rossow et al. 1989; Minnis et al. 1993b) and on the order of 15%–25% for thicker water clouds (Rossow et al. 1989).

Atmospheric transmittance and molecular scattering are computed based on the MODTRAN4 model with the U.S. standard atmospheric temperature and humidity profiles (Berk et al. 1999). Biases in retrieved cloud VIS optical depths due to neglecting atmospheric variability are small. Biases in the retrieved ε_{hc} and τ_{hc} due to neglecting atmospheric attenuation at the 11-μm channel also tend to be small. In a moist tropical atmosphere, it would lead to a positive bias of no more than a few degrees in terms of 11-μm brightness temperatures. Such a bias gives relatively small errors in ε_{hc} and τ_{hc} if T_{hc} and T_{lc} are significantly different (>20 K). The errors increase as their differences decrease, which tends to occur toward high latitudes. In such cases, the retrieval errors also become more sensitive to biases in the retrieved T_{hc} and T_{lc}.

While one can specify a surface albedo, for the demonstration purpose a constant surface albedo is set equal to 0.05. The retrieved τ_{hc} and τ_{lc} may be biased over areas of uncertain albedo, such as snow/ice-covered surfaces (polar region), sun-glint over water surfaces, and mountainous areas. Small uncertainties ($\pm$10%) in surface albedo and atmospheric properties have little impact on the retrievals when the total-column τ_{VIS} is larger than about 5. Since the retrieval of high cloud τ_{hc} relies primarily on the 11-μm and CO_2-slicing channels. Biases in surface albedo have more influence on the retrieval of low cloud τ_{lc} because its retrieval relies on the VIS channel. For example, an uncertainty of 3% in the VIS reflectance can lead to an error of 1.2 for a moderate value of $\tau_{lc} \sim 10$. In light of retrieval uncertainties, the marginal DLH retrievals with $\tau_{lc} < \Delta\tau_{lc}$ are probably single layer. The threshold $\Delta\tau_{lc}$ should depend on scene types and sun and satellite zenith angles. However, this study simply uses $\Delta\tau_{lc}$ = 1.5 for demonstrating purpose.

As the algorithm is particularly suited for high-level cirrus cloud overlapped with low-level water cloud, its success depends on a well-defined two-layer high and low cloud system. Figure 5 shows a near-global survey of the frequency distributions of the MODIS PC data (MOD06, collection 4) derived from an eight-day sampling (days 2, 6, 10, 14, 18, 22, 26, and 30) during April 2001. The frequency distributions are shown separately in 12 subpanels for each 10° latitudinal band from 60°S to 60°N over oceans (shaded) and over land (dashed lines). Also included are their corresponding 10° latitude zonal-mean overcast amounts (in parentheses). A striking bimodal distribution is seen at all latitudes, implying that the dominant cloud regimes are high and low clouds. The two cloud regimes are separated by a minimum occurrence at around 500 hPa with a wider separation in the Tropics than at higher latitudes. The

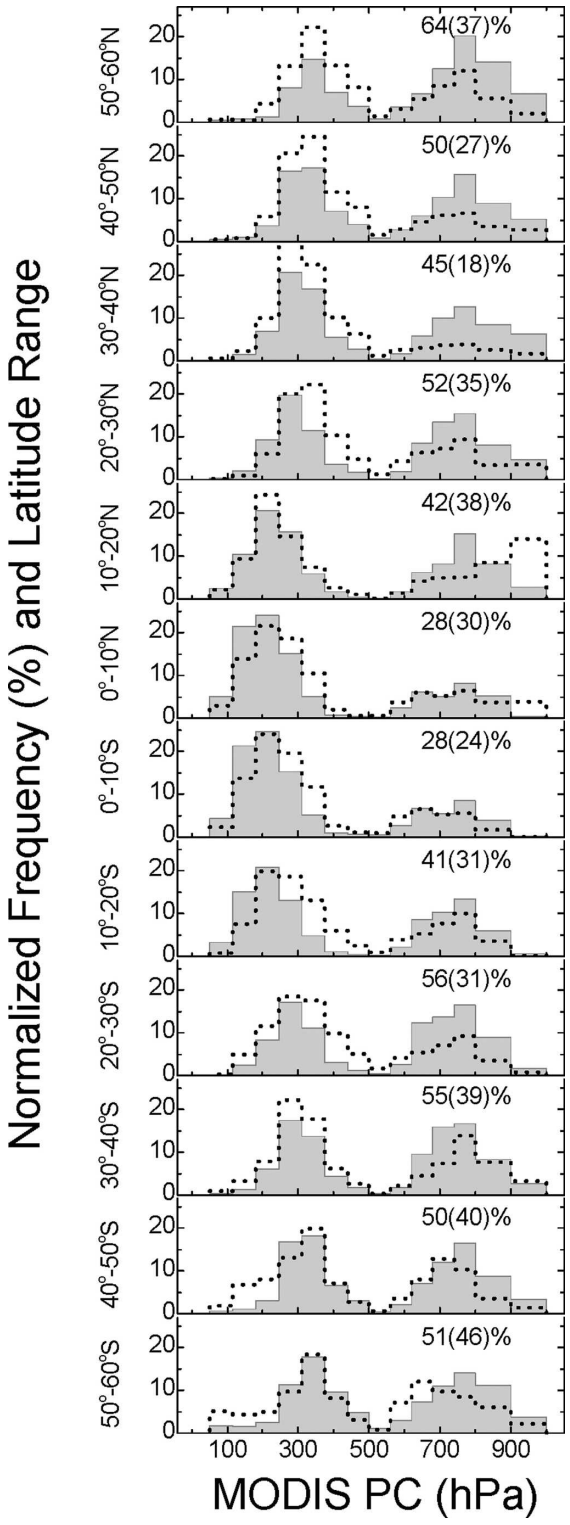

FIG. 5. MODIS (MOD06) PC frequency distributions for overcast clouds obtained from an eight-day sampling (every fourth day) during Apr 2001 for over ocean (shaded) and land (dashed lines). Results are shown for every 10° latitude region from 60°S to 60°N. The overcast cloud amounts are also indicated for ocean (land).

finding implies that the majority of cloud tops are either confined to low levels or developed to much higher levels with very few clouds toped around the 500-hPa region of the atmosphere.

A few other studies have also revealed such dominant high and low cloud regimes with minimum cloud observations in the middle atmosphere (Zuidema 1998; Comstock and Jakob 2004). In particular, Comstock and Jakob (2004) compare the ARM ground-based Active Remotely Sensed Cloud Locations (ARSCL) measurements (Clothiaux et al. 2000) with those predicted by the European Centre for Medium-Range Weather Forecasts (ECMWF) model in the tropical western Pacific over an eighth-month period between April and November of 1999. Both ground measurements and model predictions show similar cloud-height statistics that tropical clouds are generally confined to altitudes either higher than 10 km and below 2 km.

A similar general feature is also revealed over the ARM SGP region. Figure 6 compares the ARSCL (solid line) and MODIS (dotted lines) composite statistics of cloud-top frequency obtained for the entire month of April 2001 at the ARM SGP/CF location. The ARSCL data are collected within ±1 h of the *Terra*/MODIS overpass time at SGP; whereas the MODIS PC data are collected over a spatial domain of $\sim(100\ \text{km})^2$ centered at the CF. Two MODIS frequency distributions are plotted: the operational MODIS product (thin dotted line) and retrievals from this study (thick dotted line). The latter accounting for the overlapped low clouds thus produces about twice the total low cloud

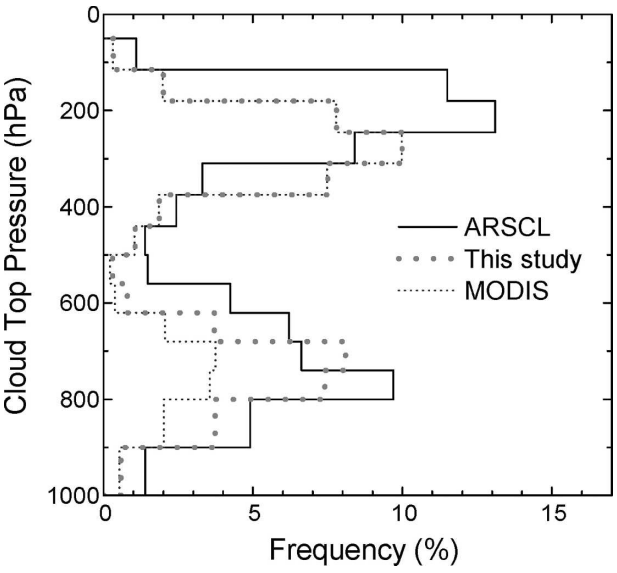

FIG. 6. Comparisons of the frequency distributions of cloud-top pressure derived from the ARM ARSCL, this study, and the operational MODIS product in Apr 2001 at the ARM SGP location.

amount comparing to the operational MODIS product. Despite the differences in temporal and spatial sampling, both ARSCL and MODIS clearly show the distinctive bimodal cloud regimes. While causes for this distinctive cloud-top vertical distribution warrant further investigation, it is beyond the scope of this study.

The finding of the bimodal high and low cloud regimes has several implications for this study. First, it implies that the high-top clouds and low-top clouds are well separated in their vertical locations so successful retrievals can be performed under most circumstances. Second, our dual-layer model can cope with the majority of multilayer cloud cases because they are dominated by the two-layer cloud configuration. Wang et al. (2000) used 20 yr of global radiosonde data to analyze cloud vertical structure and found that 42% of their clouds had more than one layer. Among them, 28% were two-layer cloud systems and 14% had three or more layers. Third, we can limit our detection and retrieval of dual-layer clouds to the high clouds with PC < 500 hPa. Below this level, the clouds are generally too thick and too low to be able to detect any additional layers.

4. Demonstration, validation, and error analyses

The outputs of our retrieval algorithm are 1) the classification of five cloud categories, namely SLH, DLH, marginal DLH, THH, and SLL, and 2) the retrievals of cloud optical properties, namely, cloud-top temperature and pressure, cloud optical depth, and emissivity. They include T_{hc}, P_{hc}, τ_{hc}, and ε_{hc} for the high cloud categories of SLH, DLH, and THH; and T_{lc}, P_{lc}, τ_{lc}, and ε_{lc} for the low cloud categories of SLL and DLL (the underlying low cloud associated with DLH). Figure 7 shows the MODIS PC product (Fig. 7a), our cloud type classification (Fig. 7b), and our retrievals of T_{hc}, τ_{hc}, T_{lc}, and τ_{lc} (Figs. 7c–f, respectively) for the granule data shown in Figs. 1a–c. Our high cloud T_{hc} and τ_{hc} are retrieved for SLH, DLH, and THH. Note that in Fig. 7d the retrieved τ_{hc} are smaller than 5 for SLH and DLH, but for THH, it is larger than 5 for the total-column τ_{VIS}. In Fig. 7e, our low cloud T_{lc} are retrieved for SLL, DLL, and THH. However, in Fig. 7f, our low cloud τ_{lc} are only retrieved for SLL and DLL and not for THH (black areas).

As a demonstration, the results of our dual-layer retrievals for overlapped high and low cloud pixels detected over the ARM SGP site (centered on 36.6°N, 97.5°W) as shown in Fig. 4a are presented in Fig. 8. Figure 8a shows the frequency distributions of the retrieved dual-layer T_{hc} and T_{lc}, along with the associated surface temperatures (T_s) from the MODIS data. The mean temperatures are ~239, 280, and 297 K for T_{hc}, T_{lc}, and T_s, respectively. Figure 8b shows the frequency distributions of the retrieved dual-layer τ_{hc} and τ_{lc}. The means are ~0.4 for τ_{hc} and ~40 for τ_{lc}. The value of τ_{lc} is similar to a 30-min mean of ~40 from the ground-based low cloud retrievals. However, the value of τ_{hc} is difficult to validate using ground-based measurements for overlapped clouds because the signals of ground-based sensors are overwhelmed by the optically thick low cloud as detected first. The backscattering signals from the upper-level much thinner cirrus clouds are greatly attenuated.

Figure 9 compares the frequency distributions of cloud-top locations derived for this case from our method (right half of the plot) within a spatial domain of ~$(100\ \text{km})^2$ and from ARSCL (left half of the plot) within a ±1 h span of the MODIS passing time at the SGP. The corresponding altitudes (left axis in kilometer) and atmospheric pressures (right axis in hPa) are from the closest sounding data obtained at Lamont, Oklahoma (~11 km from the ARM SGP central facility site), and the associated wind speed and direction are about 15 m s^{-1} (~50 km h^{-1}) from the west between 200 and 600 hPa. Both sets of measurements show a similar dual-level cloud vertical structure comprised of high clouds (>6 km) and low clouds (<4 km). The different frequencies of cloud-top occurrence are mainly attributed to the fact that ARSCL vertical pointing measurements are sampled every ten seconds while MODIS retrievals are sampled at a 5-km spatial scale. The vertical-pointing measurements are much more sensitive than the spatially averaged PC as detected by MODIS. The MODIS high cloud tops (mean ~320 hPa) are generally lower than the ARSCL data (mean ~275 hPa). Their low cloud tops are on average similar (~2.3 km or ~740 hPa). Both high cloud and low cloud top heights of the ARSCL exhibit a wider spread than those of the MODIS. The single-layer assumption made in the MODIS CO_2-slicing algorithm may be another cause for underestimating the high cloud tops due to cloud overlapping (Baum and Wielicki 1994; Menzel et al. 2002).

The algorithm is validated more extensively using both *Terra* (morning pass) and *Aqua* (afternoon pass) MODIS data between March and November 2003 that were detected as being overcast scene and having a high top PC < 500 hPa at the SGP. Table 1 presents all individual cases of our cloud identification results in comparison with the ARSCL analyses. Each ARSCL cloud top within ±5 min of the MODIS observation time is placed into one of the 1-km bins. The bins are valid if they account for more than 30% of the ARSCL measurement period. Consecutive bins are treated as

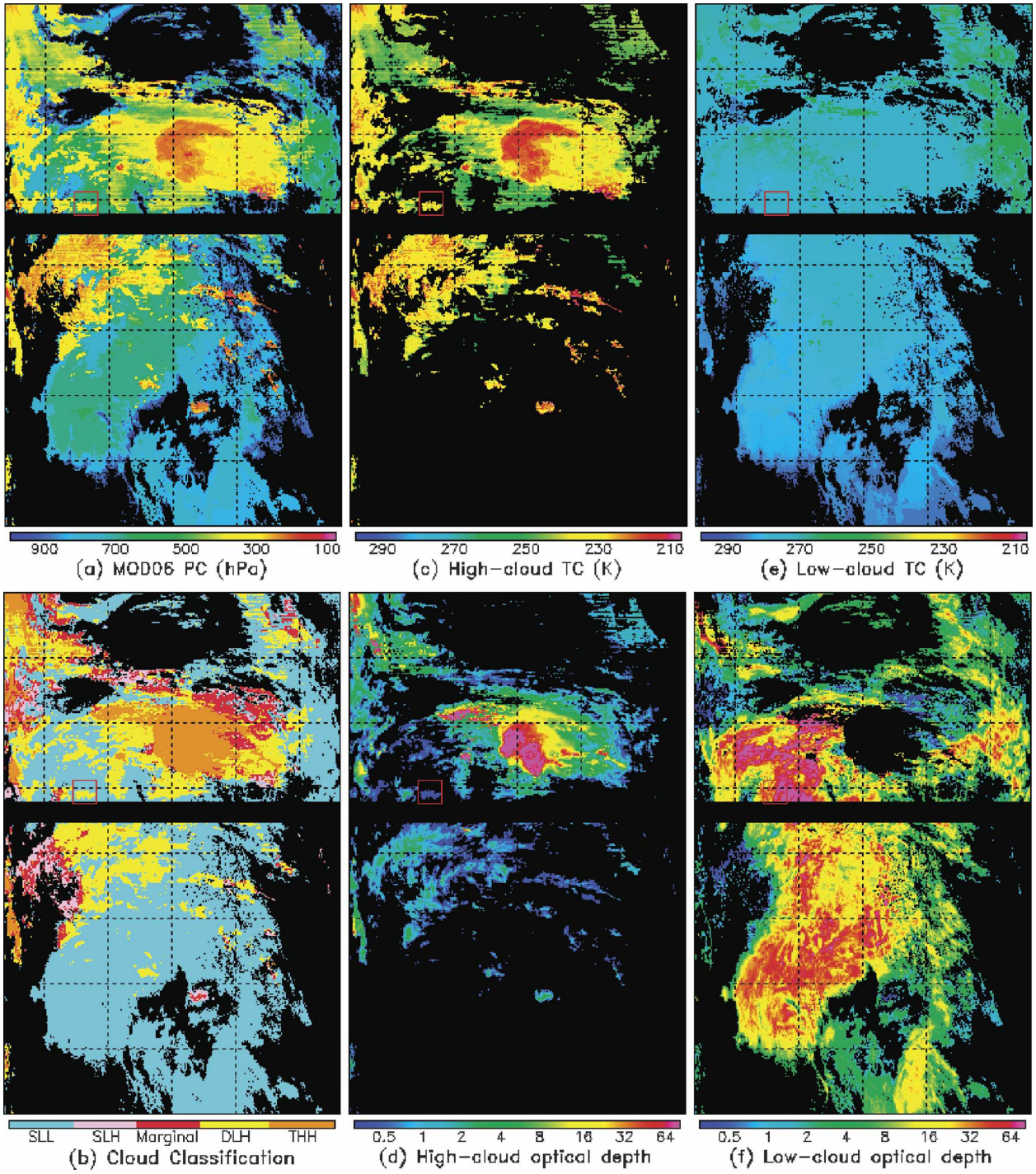

FIG. 7. (a) MODIS PC, (b) our dual-layer cloud classification, (c) T_{hc}, (d) τ_{hc}, (e) T_{lc}, and (f) τ_{lc} for the cloud image shown in Fig. 1c. The boxed area is the same as in Figs. 1a–c.

one cloud layer. In our 21 DLH cases, 17 are identified by the ARSCL as DLH, three as high clouds only, and one as low cloud only. In verifying our 20 SLH cases (including 4 marginal DLH), only 3 cases had both high and low clouds, but all 4 marginal DLH cases are found to be SLH. Also, 5 of 13 THH cases are SLH and the other 8 contained overlapped high and low clouds, for which our algorithm has identified low cloud tops from neighboring area but cannot retrieve separate τ_{hc} and τ_{lc}.

For the DLH cases, we compare the retrieved P_{hc}

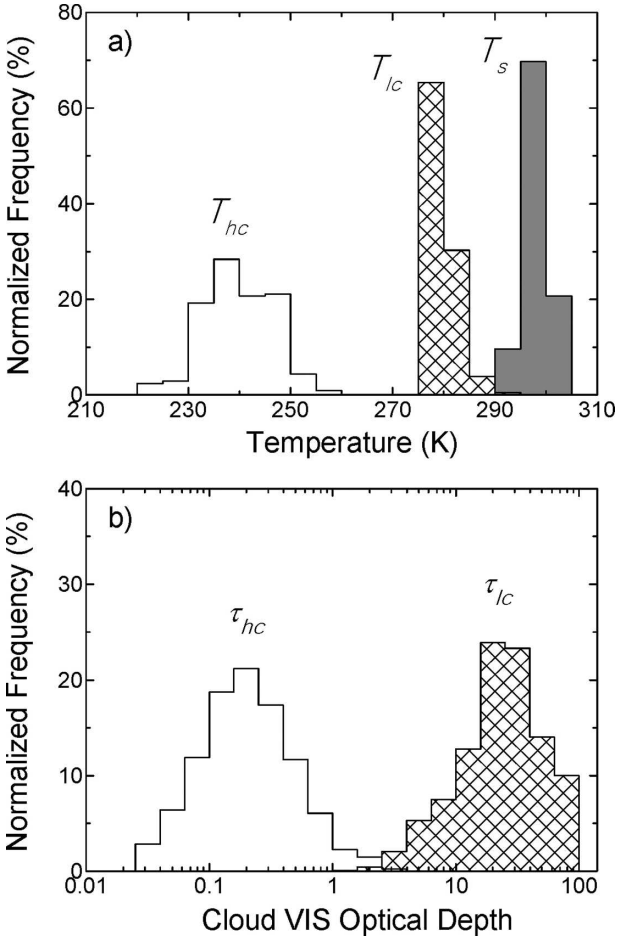

FIG. 8. Frequency distributions of (a) T_{hc}, T_{lc}, and T_s and (b) τ_{hc} and τ_{lc} for the retrievals of DLH/DLL pixels shown in Fig. 4a.

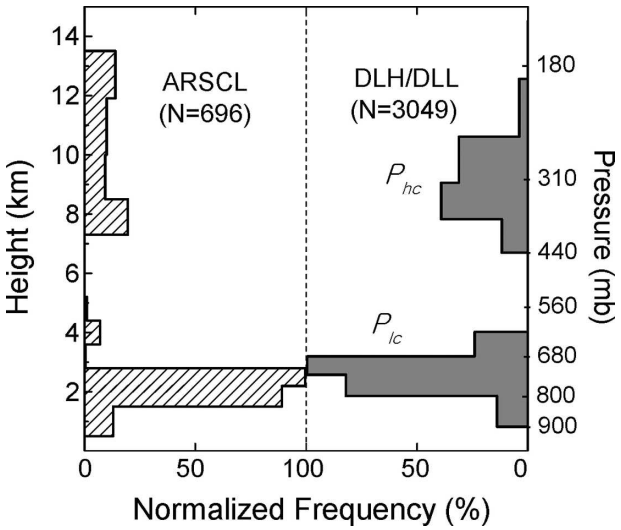

FIG. 9. Comparisons of the ARM–ARSCL (left) cloud-top heights with the (right) dual-layer retrieved PC for the overlapped cloud system observed on 2 Apr at the SGP.

and P_{lc} in Fig. 10a and T_{hc} and T_{lc} in Fig. 10b from this study against the ARSCL mean values and standard deviations. Note that for ARSCL, P_{hc} and T_{hc} are calculated for the topmost layer while P_{lc} and T_{lc} are calculated for all underlying clouds below the topmost layer. Despite that our overlapped retrievals are on average biased lower in both high and low cloud top heights, the overall comparisons exhibit reasonable agreements. As our τ_{hc} is retrieved from ε_{hc} using Eq. (5), the accuracy of τ_{hc} depends not only on T_{hc} and T_{lc} but also on the temperature differences ($\Delta T = T_{lc} - T_{hc}$) between the two layers. The retrieved τ_{hc} is less sensitive to error in T_{hc} or T_{lc} when ΔT is large, but its uncertainty increases with decreasing ΔT.

Figure 11 shows the sensitivity tests of the retrieved ε_{hc} (Fig. 11a) and τ_{hc} (Fig. 11b) based on the retrievals in Fig. 10b, which has a mean $\Delta T = 42$ K with a standard deviation of 12 K. For a mean $T_{hc} = 238$ K, mean $T_{lc} = 280$ K, mean $\tau_{hc} = 1.0$, and assuming an opaque low cloud, the sensitivity study shows that the retrieved ε_{hc} and τ_{hc} are more sensitive to errors in ΔT_{lc} than in ΔT_{hc}. The point in the upper-right corner in each panel shows the retrieval error when T_{lc} is set equal to the mean $T_s = 295$ K. It represents the error associated with the single-layer assumption for no presence of low cloud, which results in a bias error of $\Delta\varepsilon_{hc} \sim 0.2$ (Fig. 11a) and $\Delta\tau_{hc} \sim 0.8$ (Fig. 11b). According to Fig. 10b, T_{hc} and T_{lc} tend to be overestimated ($\Delta T_{hc} = 4.8$ K and rms = 10 K; $\Delta T_{lc} = 1.1$ K, and rms = 5.8 K) with large uncertainty ranges; thus ε_{hc} and τ_{hc} can be either overestimated or underestimated. In the event of a single-layer retrieval of the MODIS CO_2-slicing algorithm, P_{hc}, and so T_{hc} tend to be overestimated because of overlapped low clouds (Baum and Wielicki 1994; Menzel et al. 2002). This is because the single-layer retrieval adopts R_{clr}, which overestimates R'. Likewise, missing a middle-level cloud by our algorithm would result in an overestimation of R', leading to overestimation of ε_{hc} and τ_{hc}. Of course, if either T_{hc} or T_{lc} is underestimated, both ε_{hc} and τ_{hc} would be underestimated. Note that both ε_{hc} and τ_{hc} approach zero when $\Delta T_{lc} < -12$ K. This is because R_{lc} (or R') as shown in Eq. (5) has been largely underestimated, which becomes equivalent to the MODIS 11-μm measured radiance (R).

In case of multi-layer clouds occurring below 500 hPa, use of an averaged T_{lc} may overestimate the low cloud top and R'. However, if multiple layers occur above 500 hPa, only a single layer can be detected. Our dual-layer algorithm cannot deal with such conditions. The magnitudes of the biases also depend on τ_{hc} and τ_{lc}. The assumption of constant particle sizes for the ice and water clouds due to a lack of cloud microphysical in-

TABLE 1. Comparisons of the cloud overlap detections from this study and ARSCL for all overcast scenes identified by the MODIS at the ARM SGP/CF site during Mar–Nov 2003. The overlap detection is indicated by O; H is for high cloud only; L is for low cloud only; and TH is for thick high cloud.

MODIS passing time	This study	ARSCL
1743 UTC 17 Mar *Terra*	O	O
1917 UTC 17 Mar *Aqua*	O	O
2000 UTC 18 Mar *Aqua*	H	H
1731 UTC 19 Mar *Terra*	H	H
1954 UTC 27 Mar *Aqua*	TH	H
2000 UTC 3 Apr *Aqua*	O	O
1948 UTC 5 Apr *Aqua*	H	O
1713 UTC 15 Apr *Terra*	TH	O
1936 UTC 23 Apr *Aqua*	O	O
1954 UTC 28 Apr *Aqua*	O	O
1930 UTC 2 May *Aqua*	H	H
1719 UTC 8 May *Terra*	O	O
1725 UTC 15 May *Terra*	TH	H
1942 UTC 16 May *Aqua*	TH	O
1719 UTC 24 May *Terra*	H	H
1936 UTC 25 May *Aqua*	O	O
1725 UTC 31 May *Terra*	O	H
1743 UTC 5 Jun *Terra*	O	O
1917 UTC 5 Jun *Aqua*	O	O
1719 UTC 9 Jun *Terra*	O	H
1936 UTC 10 Jun *Aqua*	TH	O
1737 UTC 14 Jun *Terra*	H	H
1743 UTC 21 Jun *Terra*	O	O
1936 UTC 23 Jun *Aqua*	H	H
1924 UTC 28 Jun *Aqua*	H	H
1742 UTC 7 Jul *Terra*	TH	O
1712 UTC 20 Jul *Terra*	TH	O
1936 UTC 28 Jul *Aqua*	O	O
1736 UTC 1 Aug *Terra*	O	H
1742 UTC 8 Aug *Terra*	H	H
1954 UTC 18 Aug *Aqua*	O	O
1948 UTC 27 Aug *Aqua*	TH	H
1718 UTC 28 Aug *Terra*	H	H
1954 UTC 3 Sep *Aqua*	H	H
1730 UTC 11 Sep *Terra*	O	O
1718 UTC 13 Sep *Terra*	O	L
1930 UTC 23 Sep *Aqua*	H	H
1918 UTC 25 Sep *Aqua*	H	H
1736 UTC 4 Oct *Terra*	H	O
1712 UTC 8 Oct *Terra*	O	O
1743 UTC 11 Oct *Terra*	TH	O
1918 UTC 11 Oct *Aqua*	O	O
1706 UTC 17 Oct *Terra*	H	H
1930 UTC 25 Oct *Aqua*	TH	H
1718 UTC 31 Oct *Terra*	H	H
1737 UTC 5 Nov *Terra*	O	O
1743 UTC 12 Nov *Terra*	H	H
1918 UTC 12 Nov *Aqua*	H	H
2001 UTC 13 Nov *Aqua*	TH	H
1731 UTC 14 Nov *Terra*	TH	O
1936 UTC 17 Nov *Aqua*	H	O
1707 UTC 18 Nov *Terra*	O	O
1955 UTC 22 Nov *Aqua*	H	H
1713 UTC 25 Nov *Terra*	TH	O

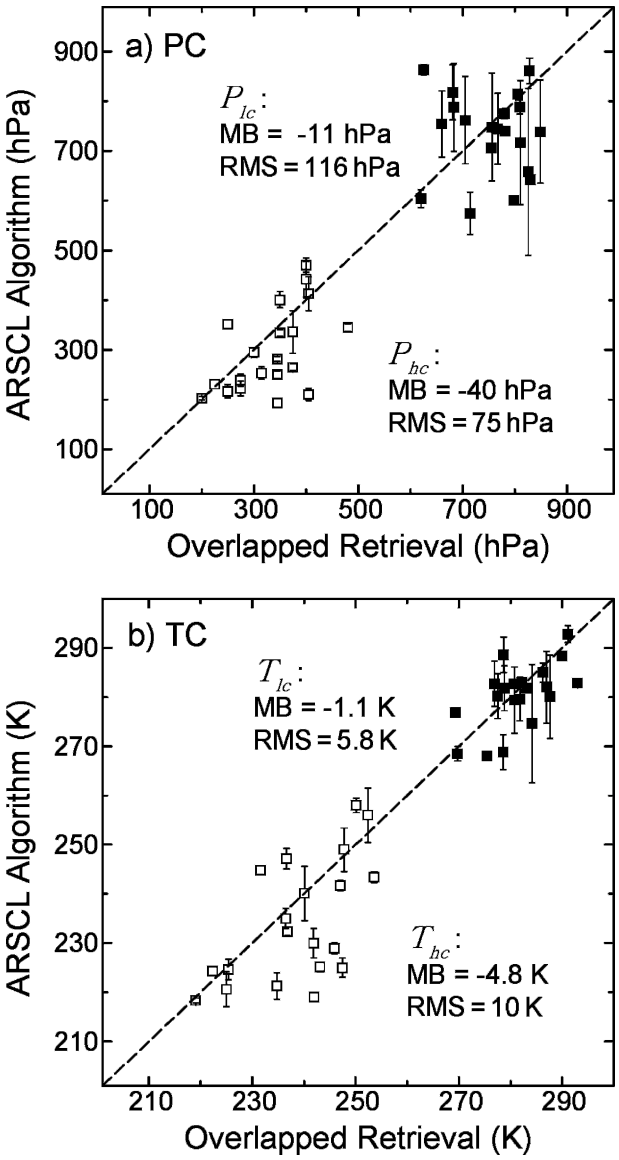

FIG. 10. Comparisons of the ground-based ARSCL analyses and the overlapped retrievals of (a) PC (hPa) and (b) TC (K) for both high cloud (open points) and low cloud (filled points) tops. The error bar indicates the standard deviation of the ±5 min ARSCL measurements. Mean biases and rms errors are given separately for high and low clouds.

formation can also contribute to the uncertainties in the retrieved τ_{hc} and τ_{lc}. While the biases in τ_{hc} may be relatively large, they often have a much smaller impact on the retrieved τ_{lc} because of the generally thicker low clouds in nature in comparison with τ_{hc} for cirrus clouds

To put this investigation and other single-layer algorithms in context, Fig. 12 compares our retrieved high cloud T_{hc} and τ_{hc} (open squares) and low cloud T_{lc} and τ_{lc} (filled squares) for the DLH cases (Fig. 12a) against the single-layer retrievals of the MODIS operational

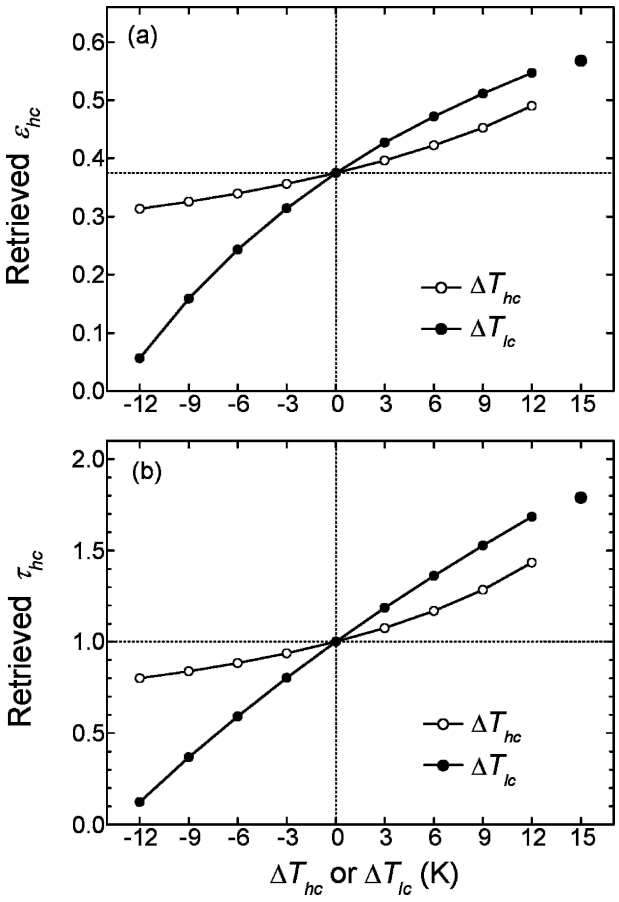

FIG. 11. Sensitivities of the retrieved (a) ε_{hc} and (b) τ_{hc} to bias errors in ΔT_{hc} (lines with open circles) and ΔT_{lc} (lines with solid circles). The point in the upper-right corner is for T_{lc} equal to T_s.

product (MOD06, collection 4) (Fig. 12b) and simulated results obtained by applying a conventional bispectral VIS–IR method (Fig. 12c). For the bispectral method, we applied the retrievals to the 0.65- and 11-μm radiances observed by MODIS. It is seen that MODIS can detect more accurately the high clouds using the CO_2-slicng method, but none of the lower clouds beneath the high clouds are identified in the operational MODIS product (Fig. 12b). One may thus mistreat the cirrus overlapping low thick clouds as optically thick high clouds. It is also seen from Fig. 12c that use of the bispectral VIS–IR method simply cannot determine either altitude of the overlapped systems. Instead, it misplaces them as middle to lower clouds somewhere in between the high and low cloud tops.

Another uncertainty raised by the conventional single-layer retrieval algorithms is that one needs to choose an ice or a water cloud model. If one chooses an ice cloud model, the underlying water clouds would overwhelm the satellite-observed radiances. On the other hand, if one chooses a water cloud model, the cirrus ice particles would contaminate the satellite-observed radiances. The resulting estimates of cloud optical depth for overlapped clouds would thus be biased positively or negatively depending on the choice of cloud phase. While our assumption of an ice cloud over a water cloud may not always be valid, it should cope with the general conditions of most overlapped cirrus and low clouds and overcome the shortcomings associated with the single-layer retrieval algorithm. Such overlapped clouds occur very frequently (Chang and Li 2005). Therefore, caution is warranted in using any cloud climatology generated by assuming a single-layer cloud only, especially in comparing cloud amounts at different vertical layers.

5. Conclusions

This study is motivated by surface and aircraft observations that reveal a large probability of high cirrus clouds coexisting with low water clouds. Because cirrus clouds are optically thin and low water clouds are often optically thicker, overlapping the two poses a major challenge for both detecting and retrieving their optical properties by satellite remote sensing. To date, all operational satellite cloud retrieval algorithms use radiative transfer models that assume a single-layer cloud. As demonstrated in this study, this single-layer assumption can incur serious biases in determining the properties of cloud-top height, temperature, optical depth, and emissivity for overlapped clouds.

In this paper, we present a dual-layer satellite cloud retrieval algorithm, which deals with overlapped cirrus and low clouds. It is designed to take advantage of the wealth of information conveyed in the MODIS data product. The dual-layer algorithm can detect the presence of overlapped cirrus and low clouds and determine the separate optical depths and cloud-top heights for the cirrus and low clouds and the cirrus IR emissivity on a pixel-level basis. It first uses a CO_2-slicing technique to determine the presence of high cloud and its cloud-top altitude and temperature. An 11-μm IR emissivity for the cirrus cloud is then calculated based on the MODIS-observed 11-μm radiance and the simulated blackbody cirrus cloud emission computed at the CO_2-slicing temperature. The IR emissivity is converted to estimate the cirrus cloud optical depth in the VIS region. The overlapped high and low cloud is initially identified for having a significant difference between the VIS-channel-retrieved cloud total-column optical depth and the IR-emissivity-converted VIS optical depth. A dual-layer cloud model is then invoked to retrieve individual cirrus and low cloud properties. The

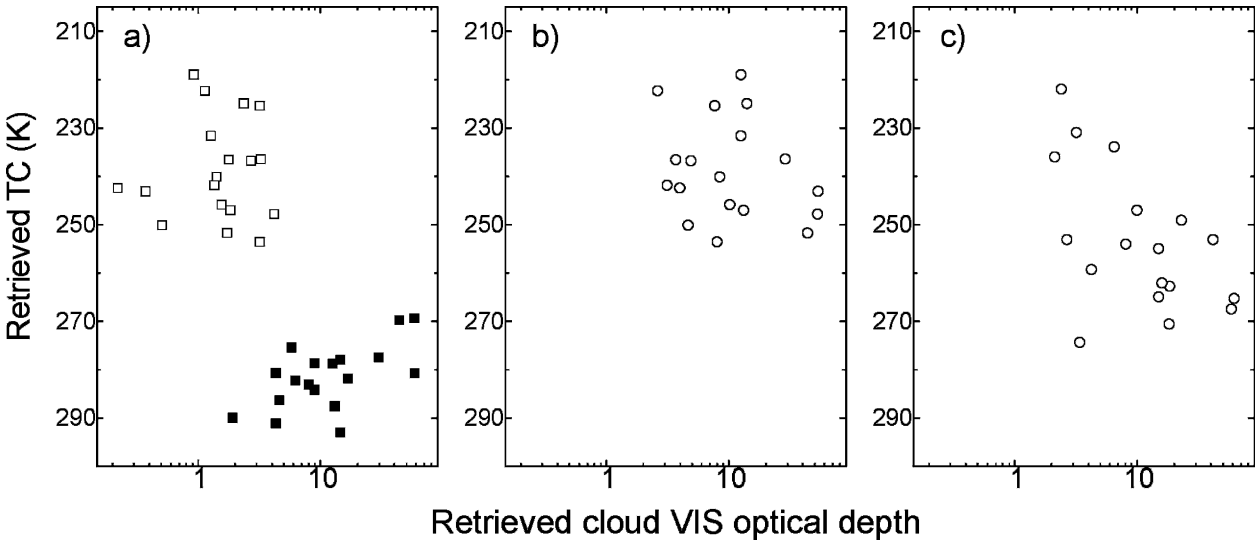

FIG. 12. Comparisons of the retrievals of TC and cloud VIS optical depth from (a) our overlapped algorithm, (b) the MODIS operational product, and (c) a conventional bispectral VIS–IR method for the DLH cases shown in Fig. 10. The retrievals in (b) and (c) assume single-layer clouds.

retrieval follows an iterative process to adjust both high cirrus and low water cloud optical depths in order to match the modeled radiances with the MODIS radiance measurements at the VIS and IR channels. The physical height of the cirrus cloud is determined by the CO_2-slicing retrieval, while that for the overlapped low cloud is determined from the average height of the clouds in neighboring MODIS pixels where single-layer low clouds are identified.

Our high cirrus and low water clouds are partitioned at the 500-hPa level, which is assumed based on a global survey of the MODIS cloud-top pressures that reveals a universal minimum of cloud-top occurrence around this level. Such a partition of high cloud and low cloud regimes is also revealed in a few other studies using ground-based measurements. High clouds with PC $<$ 500 hPa are classified into three categories: single-layer high (SLH), dual-layer high (DLH), and thick high (THH) clouds. The low clouds are thus classified into two categories: single-layer low (SLL) (PC $<$ 500 hPa) and dual-layer low (DLL).

The algorithm is designed for use with the MODIS data. One input is the MODIS CO_2-slicing retrieved cloud-top heights. Errors in this product would certainly affect our retrievals of the overlapped cloud properties. A sensitivity study shows that the retrieved cirrus τ_{hc} is not very sensitive to a bias in the MODIS CO_2-slicing temperature when the cirrus and low clouds are well separated in the atmosphere. Uncertainties and limitations associated with the new dual-layer retrieval algorithm are discussed and compared with other single-layered retrieval algorithms as used by the MODIS and conventional VIS–IR based algorithms. Preliminary validations were made through comparisons with ground-based active remote sensing data acquired in north-central Oklahoma under the U.S. Department of Energy's Atmospheric Radiation Measurement Program. The comparisons showed that this new dual-layer algorithm can overcome some major shortcomings of the conventional single-layer algorithms and can provide more accurate information on cloud-layer structure. The retrieved dual-layer cloud-top heights and optical depths showed reasonable agreement with the ground-based measurements.

Acknowledgments. The authors are grateful to both the NASA Goddard Earth Sciences (GES) Distributed Active Archived Center (DAAC) for providing the MODIS data and the Atmospheric Radiation Measurement Program (ARM) for generating and distributing ground-based cloud data. Critical comments by three anonymous reviewers help improve the quality and clarity of the paper considerably. The study is supported by the DOE ARM Grant DE-FG02-01ER63166 and a NASA Grant NNG04GE79G.

REFERENCES

Ackerman, T. P., and G. Stokes, 2003: The Atmospheric Radiation Measurement Program. *Physics Today,* **56,** 38–45.

Baum, B. A., and B. A. Wielicki, 1994: Cirrus cloud retrieval using infrared sounding data: Multilevel cloud errors. *J. Appl. Meteor.,* **33,** 107–117.

——, and J. D. Spinhirne, 2000: Remote sensing of cloud properties

using MODIS airborne simulator imagery during SUCCESS. 3. Cloud overlap. *J. Geophys. Res.,* **105,** 11 793–11 804.

——, and Coauthors, 1995: Satellite remote sensing of multiple cloud layers. *J. Atmos. Sci.,* **52,** 4210–4230.

——, V. Tovinkere, J. Titlow, and R. M. Welch, 1997: Automated cloud classification of global AVHRR data using a fuzzy logic approach. *J. Appl. Meteor.,* **36,** 1519–1540.

Berk, A., and Coauthors, 1999: MODTRAN4 v. 2.0 User's Manual. Air Force Geophysics Laboratory Tech. Rep. AFGL-TR-89-0122, 98 pp. [Available from Air Force Materiel Command, Hanscom Air Force Base, MA 01731.]

Chahine, M. T., 1974: Remote sounding of cloudy atmospheres. I. The single cloud layer. *J. Atmos. Sci.,* **31,** 233–243.

Chang, F.-L., and Z. Li, 2002: Estimating the vertical variation of cloud droplet effective radius using multispectral near-infrared satellite measurements. *J. Geophys. Res.*, **107,** 4257, doi:10.1029/2001JD000766.

——, and ——, 2005: A near-global climatology of single-layer and overlapped clouds and their optical properties retrieved from *Terra*/MODIS data using a new algorithm. *J. Climate*, in press.

Clothiaux, E. E., T. P. Ackerman, G. G. Mace, K. P. Moran, R. T. Marchand, M. Miller, and B. E. Martner, 2000: Objective determination of cloud heights and radar reflectivities using a combination of active remote sensors at the ARM CART sites. *J. Appl. Meteor.,* **39,** 645–665.

Comstock, J. M., and K. Sassen, 2001: Retrieval of cirrus cloud radiative and backscattering properties using combined lidar and infrared radiometer (LIRAD) measurements. *J. Oceanic Atmos. Technol.,* **18,** 1658–1673.

——, and C. Jakob, 2004: Evaluation of tropical cirrus cloud properties derived from ECMWF model output and ground based measurements over Nauru Island. *Geophys. Res. Lett.*, **31,** L10106, doi:10.1029/2004GL019539.

Descloitres, J. C., J. C. Buriez, F. Parol, and Y. Fouquart, 1998: POLDER observations of cloud bidirectional reflectances compared to a plane-parallel model using the International Satellite Cloud Climatology Project cloud phase functions. *J. Geophys. Res.,* **103,** 11 411–11 418.

Francis, P. N., 1995: Some aircraft observations of the scattering properties of ice crystals. *J. Atmos. Sci.,* **52,** 1142–1154.

Gonzalez, A., P. Wendling, B. Mayer, J.-F. Gayet, and T. Rother, 2002: Remote sensing of cirrus cloud properties in the presence of lower clouds: An ATSR-2 case study during the interhemispheric differences in cirrus properties from anthropogenic emissions experiment. *J. Geophys. Res.*, **107,** 4693, doi:10.1029/2002JD002535.

Hahn, C. J., and Coauthors, 1982: Atlas of simultaneous occurrence of different cloud types over the ocean. NCAR Tech. Note TN241 + STR, 209 pp. [Available from National Center for Atmospheric Research, Boulder, CO 80307.]

——, and Coauthors, 1984: Atlas of simultaneous occurrence of different cloud types over land. NCAR Tech. Note TN-241 + STR, 216 pp. [Available from National Center for Atmospheric Research, Boulder, CO 80307.]

Hale, G. M., and M. R. Querry, 1973: Optical constants of water in the 200 nm to 200 mm wavelength region. *Appl. Opt.,* **12,** 555–563.

Ho, S.-P., B. Lin, P. Minnis, and T.-F. Fan, 2003: Estimates of cloud vertical structure and water amount over tropical oceans using VIRS and TMI data. *J. Geophys. Res.*, **108,** 4419, doi:10.1029/2002JD003298.

Jin, Y., W. B. Rossow, and D. P. Wylie, 1996: Comparison of the climatologies of high-level clouds from HIRS and ISCCP. *J. Climate,* **9,** 2850–2879.

King, M. D., and Coauthors, 2003: Cloud and aerosol properties, precipitable water, and profiles of temperature and humidity from MODIS. *IEEE Trans. Geosci. Remote Sens.,* **41,** 442–458.

Lin, B., P. Minnis, B. Wielicki, D. R. Doelling, R. Palikonda, D. F. Young, and T. Uttal, 1998: Estimation of water cloud properties from satellite microwave, infrared and visible measurements in oceanic environment: 2. Results. *J. Geophys. Res.,* **103,** 3887–3905.

Liou, K. N., 1986: Influence of cirrus clouds on weather and climate processes: A global perspective. *Mon. Wea. Rev.,* **114,** 1167–1199.

Mace, G. G., E. E. Clothiaux, and T. A. Ackerman, 2001: The composite characteristics of cirrus clouds: Bulk properties revealed by one year of continuous cloud radar data. *J. Climate,* **14,** 2185–2203.

Macke, A., 1993: Scattering of light by polyhedral ice crystals. *Appl. Opt.,* **32,** 2780–2788.

Menzel, W. P., D. P. Wylie, and K. I. Strabala, 1992: Seasonal and diurnal changes in cirrus clouds as seen in four years of observations with the VAS. *J. Appl. Meteor.,* **31,** 370–385.

——, B. A. Baum, K. I. Strabala, and R. A. Frey, 2002: Cloud top properties and cloud phase algorithm theoretical basis document: ATBD-MOD-04. 61 pp. [Available online at http://modis-atmos.gsfc.nasa.gov/_docs/atbd_mod04.pdf.]

Minnis, P., D. F. Young, K. Sassen, J. M. Alvarez, and C. J. Grund, 1990: The 27–28 October 1986 FIRE IFO cirrus case study: Cirrus parameter relationships derived from satellite and lidar data. *Mon. Wea. Rev.,* **118,** 2402–2425.

——, K.-N. Liou, and Y. Takano, 1993a: Inference of cirrus cloud properties using satellite-observed visible and infrared radiances. Part I: Parameterization of radiance field. *J. Atmos. Sci.,* **50,** 1279–1304.

——, P. W. Heck, and D. F. Young, 1993b: Inference of cirrus cloud properties using satellite-observed visible and infrared radiances. Part II: Verification of theoretical cirrus radiative properties. *J. Atmos. Sci.,* **50,** 1305–1322.

Mishchenko, M. L., W. B. Rossow, A. Macke, and A. A. Lacis, 1996: Sensitivity of cirrus cloud albedo, bidirectional reflectance, and optical thickness retrieval accuracy to ice-particle shape. *J. Geophys. Res.,* **101,** 16 973–16 985.

Ou, S. C., K. N. Liou, and B. A. Baum, 1996: Detection of multilayer cirrus cloud systems using AVHRR data: Verification based on FIRE-II IFO composite measurements. *J. Appl. Meteor.,* **35,** 178–191.

Pavolonis, M. J., and A. K. Heidinger, 2004: Daytime cloud overlap detection from AVHRR and VIIRS. *J. Appl. Meteor.,* **43,** 762–778.

Platnick, S., M. D. King, S. A. Ackerman, W. P. Menzel, B. A. Baum, J. C. Riedi, and R. A. Frey, 2003: The MODIS cloud products: Algorithms and examples from *Terra*. *IEEE Trans. Geosci. Remote Sens.,* **41,** 459–473.

Platt, C. M. R., and G. L. Stephens, 1980: The interpretation of remotely sensed high cloud emittances. *J. Atmos. Sci.,* **37,** 2314–2322.

Rossow, W. B., and R. A. Schiffer, 1991: ISCCP cloud data products. *Bull. Amer. Meteor. Soc.,* **72,** 2–20.

——, and ——, 1999: Advances in understanding clouds from ISCCP. *Bull. Amer. Meteor. Soc.,* **80,** 2261–2287.

——, L. C. Garder, and A. A. Lacis, 1989: Global, seasonal cloud variations from satellite radiance measurements. Part I: Sensitivity of analysis. *J. Climate,* **2,** 419–462.

Sassen, K., Z. Wang, C. M. R. Platt, and J. M. Comstock, 2003: Parameterization of infrared absorption in midlatitude cirrus clouds. *J. Atmos. Sci.,* **60,** 428–433.

Sheu, R.-S., J. A. Curry, and G. Liu, 1997: Vertical stratification of tropical cloud properties as determined from satellite. *J. Geophys. Res.,* **102,** 4231–4245.

Smith, W. L., and C. M. R. Platt, 1978: Comparison of satellite-deduced cloud heights with indications from radiosonde and ground-based laser measurements. *J. Appl. Meteor.,* **17,** 1796–1802.

Stephens, G. L., and Coauthors, 2002: The CLOUDSAT mission and the A-Train. *Bull. Amer. Meteor. Soc.,* **83,** 1771–1790.

Tian, L., and J. A. Curry, 1989: Cloud overlap statistics. *J. Geophys. Res.,* **94,** 9925–9935.

Wang, J., W. B. Rossow, and Y.-C. Zhang, 2000: Cloud vertical structure and its variations from a 20-year global rawinsonde dataset. *J. Climate,* **13,** 3041–3056.

Warren, S. G., 1984: Optical constants of ice from ultraviolet to the microwave. *Appl. Opt.,* **23,** 1206–1225.

——, C. J. Hahn, and J. London, 1985: Simultaneous occurrence of different cloud types. *J. Climate Appl. Meteor.,* **24,** 658–667.

Wielicki, B. A., and J. A. Coakley Jr., 1981: Cloud retrieval using infrared sounder data: Error analysis. *J. Appl. Meteor.,* **20,** 157–169.

Wylie, D. P., and W. P. Menzel, 1989: Two years of cloud cover statistics using VAS. *J. Climate,* **2,** 380–392.

——, and ——, 1999: Eight years of high cloud statistics using HIRS. *J. Climate,* **12,** 170–184.

——, ——, H. M. Woolf, and K. I. Strabala, 1994: Four years of global cirrus cloud statistics using HIRS. *J. Climate,* **7,** 1972–1986.

Zuidema, P., 1998: The 600–800-mb minimum in tropical cloudiness observed during TOGA COARE. *J. Atmos. Sci.,* **55,** 2220–2228.